RSC Advances

PAPER

Nitrogen-doped graphene with high nitrogen level *via* a one-step hydrothermal reaction of graphene oxide with urea for superior capacitive energy storage†

Li Sun, Lei Wang, Chungui Tian, Taixing Tan, Ying Xie, Keying Shi, Meitong Li and Honggang Fu*

Nitrogen-doped graphene nanosheets (NGS) with the nitrogen level as high as 10.13 atom% were synthesized *via* a simple hydrothermal reaction of graphene oxide (GO) and urea. N-doping and reduction of GO were achieved simultaneously under the hydrothermal reaction. In the fabrication, the nitrogen-enriched urea plays a pivotal role in forming the NGS with a high nitrogen level. During the hydrothermal process, the N-dopant of urea could release NH_3 in a sustained manner, accompanied by the released NH_3 reacting with the oxygen functional groups of the GO and then the nitrogen atoms doped into graphene skeleton, leading to the formation of NGS. The nitrogen level and species could be conveniently controlled by easily tuning the experimental parameters, including the mass ratio between urea and GO and the hydrothermal temperature. Remarkably, in 6 M KOH electrolyte, the synthesized NGS with both high nitrogen (10.13 atom%) and large surface area (593 m^2 g^{-1}) exhibits excellent capacitive behaviors (326 F g^{-1}, 0.2 A g^{-1}), superior cycling stability (maintaining initial capacity even) and coulombic efficiency (99.58%) after 2000 cycles. The energy density of 25.02 Wh kg^{-1} could be achieved at power density of 7980 W kg^{-1} by a two-electrode symmetric capacitor test. A series of experiments results demonstrated that not only the N-content but also the N-type are very significant for the capacitive behaviors. In more detail, the pyridinic-N and pyrrolic-N play mainly roles for improving pseudo-capacitance by the redox reaction, while quaternary-N could enhance the conductivity of the materials which is favorable to the transport of electrons during the charge/discharge process. Hence, the approach in this work could provide a new way for preparing NGS materials which could be used as advanced electrodes in high performance supercapacitors.

1. Introduction

During the past few decades, supercapacitors, also known as electrochemical capacitors (ECs), are increasingly important due to their intrinsic features of high power and energy density, ultra-long cycle life and low maintenance cost, which make them serve as promising candidates in many fields, such as hybrid electric vehicles, mobile electronics and other power-supply devices.[1,2] Based on the charge-storage mechanism, ECs can be divided into two categories, namely pseudo-capacitors and electrical double-layer capacitors (EDLCs).[3] Redox-active materials, such as transition-metal hydroxide/oxides[4,5] and conducting polymers,[6] are essential materials for pseudo-capacitors due to their high specific capacitance though Faradaic reactions. However, the poor cycling stability, electrical conductivity and high cost would limit their further applications. On the other hand, carbon-based materials, such as activated carbons (ACs) and carbon nanotubes (CNTs), are current electrode materials for EDLCs owing to their nature of good chemical stability and availability.[7–11] Though ACs possess large specific surface area and abundant micropores, they still suffer from capacitance degradation owing to lagged ion transport within their closed or tortuous pore structure.[12] CNTs that have high electronic conductivity and excellent structure but their electrochemical performances are still low for an actual device application due to their low surface areas.[13]

Graphene, a flexible two-dimensional (2D) carbon material, is regarded as a promising and attractive electrode for potential application in ECs, because of its high electrical conductivity and theoretical surface area. However, the extremely low intrinsic capacitance of graphene nanosheets (GS) is not enough to fulfil the demand of commercial applications as independent energy storage devices.[14,15] Recently, efforts have been reported introducing heteroatom of nitrogen into GS for modulation of the electron donor or acceptor properties intrinsically, so as to improve the specific capacitance and cycle ability of nitrogen-doped graphene nanosheets (NGS).[16,17] Up to now, several approaches have been employed to synthesize NGS. Chemical

Key Laboratory of Functional Inorganic Material Chemistry, Ministry of Education of the People's Republic of China, Heilongjiang University, Harbin, 150080, P. R. China. E-mail: fuhg@vip.sina.com; Fax: (+86) 451 8666 1259; Tel: (+86)451 8660 9115
† Electronic supplementary information (ESI) available. See DOI: 10.1039/c2ra01367c

vapor deposition (CVD),[18] arc discharge,[19] and nitrogen plasma process[20] are reliably and straightforward methods to fabricate single- and few-layers NGS. However, these processes suffered from rigorous conditions and complicated equipment, accompanied by low-yields and high-cost. In addition, the nitrogen precursors of pyridine and the NH_3 are also adverse to the environment and the subsequent treatments. Electrothermal reaction[21] or thermal annealing graphite oxide (GO) with NH_3[22] can indubitably produce a high-throughput of the NGS. Nevertheless, the N-doped level in as-prepared NGS was merely of 5 wt%. Recently, hydrothermal and solvothermal reactions have been used as effective approaches to fabricate NGS with a high nitrogen level.[23] Yoon and co-workers developed a novel hydrothermal process in the presence of hydrazine and ammonia to fabricate NGS. Unfortunately, the N_2H_4 can not be stored due to its toxicity and risk of explosion. Additionally, Bao's group synthesized NGS with an exceptional nitrogen level of up to 13 at% (N C^{-1} = 16.4%) by a solvothermal reaction between tetrachloromethane and lithium nitride. Although the high-cost and rigorous reaction conditions may limit further potential applications, the obtained NGS exhibited an outstanding performance in the oxygen reduction reaction of fuel cell, as expected. As known, the performance of the NGS in ECs is related not only to the nitrogen level, but also to the types of the nitrogen. In detail, pyridinic-N and pyrrolic-N play key roles in enhancing the specific capacitance of N-doped materials due to their pseudo-capacitive contribution, while quaternary-N could enhance the conductivity of the materials.[24] Moreover, the high electrochemical performance is also attributed to the large surface areas which can facilitate electrolyte penetration and ion transport.[25] Therefore, it is both urgent and indispensable to develop simple and efficient approaches to prepare NGS with high nitrogen content, appropriate nitrogen species and large surface areas.

In this study, we demonstrated a facile and effective one-step hydrothermal reaction to simultaneous N-doping and reduce GO under the assistance of urea (Scheme 1). During the hydrothermal reaction, N-doping and reduction of GO were achieved simultaneously. In this process, urea can gradually release NH_3 that continually reacts with the oxygen functional groups of GO, which is favorable for doping of high-level nitrogen into graphene skeleton. Importantly, the nitrogen content and types could be tuned by controlling the experimental conditions, including the mass ratio between urea and GO, hydrothermal temperature. The highest nitrogen content in this approach could be up to 10.13 atom%. Moreover, the synthesized NGS has a specially large surface area of 593 m^2 g^{-1}, which is much higher than those of the NGS materials synthesized by other methods previously.[16,23,26] Most importantly, the NGS could act superior electrode materials for supercapacitors with an excellent

capacitance, outstanding cycling stability, coulombic efficiency and high power and energy density, implying the great potential of this material as advanced electrodes in ECs. In addition, the urea is regarded as a kind of abundant, low-cost, nitrogen-enriched and easily reserved material. Thus, this method can be widely applied to the synthesis of NGS for practical applications as outstanding energy storage materials.

2. Experimental

2.1. Synthesis of Graphene Oxide (GO)

GO sheets were synthesized from expandable graphite flakes by a modified Hummers method.[27] Briefly, expandable graphite (2.0 g) was combined with 50 mL concentrated sulfuric acid in a 250 mL beaker under vigorous agitation at room temperature. Afterwards, sodium nitrate (2.0 g) and potassium permanganate (6.0 g) were slowly poured into the beaker in a sequence. Next, the mixture was heated at 35 °C for 24 h. After that, 80 mL of distilled water was added into the solution. 5 min later, 20 mL of 30% H_2O_2 was dropped into the reaction system. Finally, the product was washed with HCl solution and then washed three times with water. The resulting solid was dispersed in water by ultrasonication to make a GO aqueous dispersion with the concentration of about 4 mg mL^{-1}.

2.2. Preparation of the N-doped graphene nanosheets

The N-doped graphene nanosheets with high nitrogen content were synthesized through a one-pot hydrothermal process using urea as the chemical dopant in the presence of GO aqueous dispersion. Typically, 10 mL GO (40 mg) aqueous dispersion was diluted with 25 mL of deionized water, and then a given amount of urea was added into the GO dispersion under sonication for 3 h. After that, the solution was sealed in a 50 mL Teflon-lined autoclave and maintained at 180 °C for 12 h. The solids (N-doped graphene sheets) were filtered and washed with distilled water several times. Finally, the collected sample, denoted as NGS-1, was drying in a vacuum oven at 80 °C. A series of experiments were performed to investigate the effects of experimental parameters (urea doses, hydrothermal temperature) on the micro-structure of NGS. The synthesis conditions for different samples are listed in Table S1, ESI.† For comparison, reduced GO (RGO) was also prepared under the same experimental parameters but without adding the urea into the GO aqueous dispersion.

2.3. Characterization

The microstructure and morphology of the products were investigated by scanning electron microscopy (SEM, Hitachi S-4800) with an acceleration voltage of 5 kV, transmission electron microscopy (TEM, JEM-2100) with an acceleration voltage of 200 kV and atomic force microscopy (AFM, Agilent Technologies 5100, operating in tapping mode) measurements, respectively. X-ray diffraction (XRD) patterns were obtained on a Rigaku D/max-IIIB diffractometer using Cu-Kα (λ = 1.5406 Å) at step scan 0.02° from 5° to 80°. The accelerating voltage and the applied current were 40 kV and 20 mA. The nitrogen adsorption/desorption isotherms were measured at 77 K using a Micromeritics Tristar II. X-ray photoelectron spectroscopy

Scheme 1 Schematic procedure for preparation of NGS.

(XPS) analysis was performed on a VG ESCALAB MK II with an MgKa (1253.6 eV) achromatic X-ray source. Elemental analysis was carried out with a conventional combustion method (CHN, varioMLCRO) based on the burn-off mass of the sample and on the analysis of the evolved gases using a thermal conductivity detector. Oxygen content was calculated as a difference between 100% and the sum of C + H + N, assuming that ash is not present. The assumption results in the approximated values of the oxygen content.

2.4. Electrochemical measurements

The three-electrode system was used to measure the performance of the graphene-based materials in 6 M KOH aqueous electrolyte. The working electrodes were prepared by mixing the as-prepared samples, poly (tetrafluoroethylene) (PTFE) and carbon black at the weight ratio of 90 : 5 : 5. The mixtures (10 mg) were coated onto a 1 cm × 1 cm nickel foam current collector, and dried at 60 °C for 8 h. Platinum foil and saturated calomel electrode (SCE) were used as counter electrode and reference electrode, respectively. Electrochemical impedance spectroscopy (EIS) measurements were carried out by applying an AC voltage with 5 mV amplitude in a frequency range from 0.01 Hz to 100 kHz at the open circuit potential. The cyclic voltammograms (CV) curves were measured by BAS100B electrochemical workstation. The constant current charge-discharge capacitance test was performed with a CHI 660D electrochemical workstation. The specific capacitance of the electrode can be calculated from the galvanostatic charge and discharge curves according to the following equation:[28]

$$C = \frac{I\Delta t}{m\Delta V} \qquad (1)$$

Where C is the specific capacitance (F g^{-1}), I is the charge/discharge current density (A g^{-1}), Δt is the discharge time (s), m is the mass of active material in the electrode (g), and ΔV indicates the voltage change after a full charge or discharge.

The coulombic efficiency was calculated using the following equation:[28]

$$\eta = \frac{t_d}{t_c} \times 100 \qquad (2)$$

Where t_c and t_d represent the time of charge and discharge, respectively.

The two-electrode symmetric cell was conducted in a CR2025 coin-type cell, with a glassy fibrous separator between the pellets. Charge and discharge measurements between −1.1 and 0 V were carried out by LAND CT2000 (Wuhan Jinnuo Electronics, Ltd., Wuhan, China) at different current densities. The specific capacitance, and power and energy density were calculated based on the total mass of anode and cathode materials. Gravimetric capacitance from galvanostatic charge/discharge was calculated using the formula:[29]

$$C_{carbon} = \frac{4I}{m\mathrm{d}V/\mathrm{d}t} \qquad (3)$$

I is the charge/discharge current density (A g^{-1}), m (g) is the total mass of anode and cathode materials and dV/dt was calculated from the slope obtained by fitting a straight line to the discharge curve over the range of V_{max} to 1/2 V_{max}.

The energy density was calculated as the following equation:[29]

$$E_{cell} = \frac{1}{8}CV^2 \qquad (4)$$

where C is the carbon-based materials capacitance and V is the cell-operation potential.

The maximum power density was calculated by using the formula:[12]

$$P_{max} = \frac{V^2}{4R_{ESR}m} \qquad (5)$$

Where R_{ESR} is the equivalent series resistance and m (g) is the total mass for both carbon electrodes.

3. Results and discussion

The nanostructure of the as-prepared NGS-1 synthesized at 180 °C for 12 h hydrothermal reduction with a mass ratio between urea and GO of 300 : 1, was investigated by scanning electron microscopy (SEM) and transmission electron microscopy (TEM). The SEM image (Fig. 1a) shows complex three-dimensional (3D) porous NGS with stacked and overlapped structures and the pore walls cross-linking with each other. Also, the flame-like NGS were mechanically flexible, as shown in Fig. 1b, which should be a crucial factor for forming the coalesced 3D macrostructures. The TEM image (Fig. 1c) showed NGS-1 with a structure of stacked and wrinkled nanosheets. Meanwhile, NGS-1 was estimated to be composed of 8-layer based on the analysis of the HRTEM image (Fig. 1d). The typical AFM image and thickness analysis of the NGS-1 sample (Fig. 1e and 1f) show the height of NGS-1 is about 4.0–4.5 nm. Nevertheless, the RGO synthesized under the same experimental parameters but without urea are partly aggregated due to the
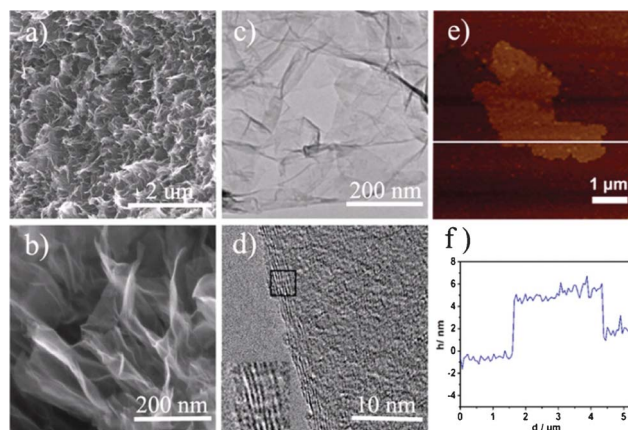

Fig. 1 a, b) SEM, c) TEM and d) HR-TEM images of the NGS-1(mass ratio of urea/GO is 300 : 1, 180 °C, 12 h); e) Representative AFM image and f) corresponding thickness analysis taken around the white line in e) reveal a thickness of 4–4.5 nm for NGS-1.

strong Van der Waals forces among individual graphene nanosheets (Fig. S1, ESI†).

The nitrogen adsorption/desorption isotherm of the synthesized NGS-1 sample was shown in Fig. 2a, and the type IV nitrogen adsorption branch associated with a H2 hysteresis loop was observed. The BET surface area and total pore volume are 593 $m^2 g^{-1}$ and 0.092 $cm^3 g^{-1}$, respectively. The corresponding pore size distribution calculated by the Barrett–Joyner–Halenda (BJH) method is about 3 nm (inset of Fig. 2a). However, the surface area of the RGO is only 260 $m^2 g^{-1}$ (see Fig. S2, ESI†), which is much lower than that of the NGS-1 sample, indicating that the N-doping indeed effectively prevents the aggregation of adjacent graphene nanosheets.[30]

The X-ray diffraction (XRD) patterns of the original GO and NGS-1 were displayed in Fig. 2b. The diffraction peak located at $2\theta = 10.1°$ is attributed to the (002) crystalline plane of GO and the corresponding calculated interlayer spacing is about 0.87 nm. However, the peak at $2\theta = 10.1°$ entirely disappeared after hydrothermal reaction, and a broad diffraction peak around 25° of the graphite (002) plane was observed for the synthesized NGS-1 sample, indicating the framework of the reduced sample was composed of few-layer stacked graphene nanosheets.[23] Besides, the interlayer distance was reduced from 0.87 nm of GO to 0.36 nm of NGS-1, which certified the recovery of π-conjugated system after the reduction of GO.

X-ray photoelectron spectroscopic (XPS) and elemental analysis (CHN) were carried out to evaluate the chemical composition of NGS samples. The typical XPS spectra of the as-prepared NGS-1 and RGO samples are displayed in Fig. 3a. The N 1s peak is not obvious for RGO; however, the N1s peak in the NGS-1 sample could be divided into three components, as shown in Fig. 3b, implying that the N atoms are in the three different valence states doped into the graphene skeleton. As can be seen, pyridinic-N (N1, 398.1 eV) contributes to the π-conjugated system with a p-electron in the graphene layers; pyrrolic-N (N2, 399.5 eV) refers to the N atom contributing two p-electrons to the π system, which is ascribed to the contribution of pyridone and pyrrol functionalities; quaternary-N (N3, 401.6 eV) is derived from the N atoms that replace the C atoms in graphene hexagonal-ring.[31]

As shown in Fig. 3c, the C1s core level peak of the RGO shows one main peak at 284.4 eV (C–C), three small peaks at higher binding energy indicate the existence of oxygen groups, including C–OH at 285.5 eV, C=O at 287.1 eV, and C–C=O at 289.0 eV,[32] which decrease considerably after hydrothermal reaction of the GO (Fig. S3, ESI†). Moreover, the oxygen content in RGO was
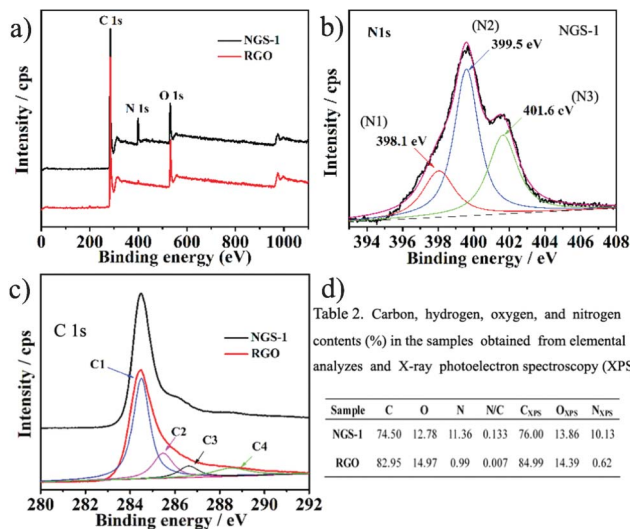
Fig. 3 a–c) XPS wide spectra, N1s spectra and C1s spectra of the synthesized NGS-1 and RGO samples, respectively; d) Elemental content and chemical composition in NGS-1 and RGO samples tested by elemental analysis and XPS.

Table 2. Carbon, hydrogen, oxygen, and nitrogen contents (%) in the samples obtained from elemental analyzes and X-ray photoelectron spectroscopy (XPS)

Sample	C	O	N	N/C	C_{XPS}	O_{XPS}	N_{XPS}
NGS-1	74.50	12.78	11.36	0.133	76.00	13.86	10.13
RGO	82.95	14.97	0.99	0.007	84.99	14.39	0.62

reduced sharply from 38.54 atom% to 13.86 atom%, further revealing that the GO could be reduced to graphene during the hydrothermal progress. For the C1s spectrum of NGS-1 as shown in Fig. 3c, the main peak at 284.4 eV is related to the C–C, implying that most of the C atoms in the NGS-1 are arranged in a conjugated honeycomb lattice. Additionally, the other two peaks located at 285.7 and 286.6 eV are ascribed to C=N and C–N, respectively, and originate from when the oxygen atoms of GO are substituted by N atoms.[33] It should be noted that the peak of C=O is overlaid with C–N around the binding energy of 287.1 ± 0.5 eV.[34] However, the peak around 286.5 eV for C=O or C–N increased significantly after N-doping, implying that NGS can be successfully prepared by the hydrothermal reaction between GO and urea. Fig. 3d shows the mass and atom percentages of nitrogen, carbon, and oxygen in RGO and NGS-1, respectively. The CHN analysis reveals bulk composition of NGS-1 with a nitrogen content of 11.36 wt%, which is similar to the results of XPS(10.13 atom%).

Remarkably, the nanostructure and surface functionalities of the synthesized NGS materials can be tailored by controlling the synthetic conditions, including urea doses and hydrothermal temperature. From the SEM images shown in Fig. S4 and Fig. S5, see ESI,† the NGS materials with coalesced 3D porous morphologies were also successfully synthesized no matter how the mass ratio between urea and GO or the hydrothermal temperature changed. Firstly, the NGS products derived from different mass ratio between urea and GO have been studied. As a result, it is obvious that more nitrogen atoms (especially N2 and N3) could be doped into the graphene networks along with the increase of urea dose from the XPS and CHN analyses, as shown in Table 1. However, the nitrogen content in NGS products does not increase when the mass ratio between the urea dose and GO increased to 300 : 1, indicating the NGS with the highest nitrogen content could be prepared under a proper mass ratio between the urea dose and GO. Besides, the S_{BET} (Table 1) is firstly increased with the increasing urea dose, and a highest

Fig. 2 a) Nitrogen adsorption/desorption isotherm and the corresponding pore size distribution (inset) of the synthesized NGS-1sample; b) XRD patterns of the synthesized NGS-1 sample and GO powder.

Table 1 S_{BET} and elemental analyses of the as-prepared materials under different synthetic conditions, S_{BET} was calculated from nitrogen adsorption/desorption isotherms; the N contents were determined using combustion CHN method and XPS measurement, additionally, the C and O contents were obtained using XPS

Samples	Mass ratio of the urea and GO	Hydrothermal temperature	S_{BET} (m^2 g^{-1})	C_{XPS} (atom%)	O_{XPS} (atom%)	N_{CHN} (wt%)	N_{XPS} (atom%)	N1 398.1 eV	N2 399.5 eV	N3 401.6 eV
RGO	0 : 1	180 °C	260	84.99	14.39	0.99	0.62	—	—	—
NGS-1	300 : 1	180 °C	593	76.00	13.86	11.36	10.13	2.21	5.11	2.77
NGS-2	100 : 1	180 °C	502	81.02	14.02	6.87	4.96	1.76	2.38	0.82
NGS-3	200 : 1	180 °C	527	80.27	13.72	7.35	6.01	1.93	2.62	1.38
NGS-4	400 : 1	180 °C	571	79.25	11.81	9.86	8.94	2.74	4.35	2.41
NGS-5	500 : 1	180 °C	544	79.78	11.77	9.79	8.45	2.91	4.59	0.97
NGS-6	300 : 1	160 °C	373	77.72	15.91	8.00	6.37	1.84	3.47	1.05
NGS-7	300 : 1	170 °C	460	77.75	14.40	9.29	7.85	2.88	3.87	1.09
NGS-8	300 : 1	190 °C	413	81.98	10.73	8.83	7.29	2.36	4.09	0.85

S_{BET} of 593 m g^{-1} of NGS is obtained when the mass ratio between urea and GO is up to 300 : 1. However, the S_{BET} value starts to decrease if the urea dose is further increased, and the smaller S_{BET} value is 544 m^2 g^{-1} in the present experiment (the mass ratio between urea and GO is up to 500 : 1). The change tendency of S_{BET} is similar to that of the nitrogen content, because the existence of nitrogen functionalities (nitrogen level) could inhibit the aggregation of graphene nanosheets.[30] Additionally, the effect of hydrothermal temperature on the nanostructure and surface functionalities of the synthesized NGS is also very obvious. As shown in Table 1, it is important to note that more N2 and N3 could be doped into the graphene networks with an increase of the hydrothermal temperature from 160 °C to 180 °C. When the reaction temperature was up to 190 °C, the total nitrogen content and the N3 type decreased instantly. Meanwhile, the oxygen level lowers gradually with the increase of reaction temperature. Furthermore, the change tendency of S_{BET} (Table 1) along with the hydrothermal temperature is similar to that of nitrogen content. Based on the above analyses, it was deduced that the types and content of nitrogen in the as-prepared NGS products could be controlled by tuning the mass ratio between urea and GO and hydrothermal temperature.

To investigate the possible nitrogen insertion pathway in graphene sheets, XPS N1s spectra of the NGS products prepared at different hydrothermal reaction times were studied (Fig. 4), and the possible formation mechanism is shown in Scheme 2. From the XPS N1s spectrum shown in Fig. 4a, N1 and N2 are the main species during the initial stage of the hydrothermal process, (4 h). Considering that urea releases NH$_3$ in a sustained

manner at a relatively slower rate, and the NH$_3$ persistently reacts with the oxygen functional groups (carboxylic acid and hydroxyl species) present on the graphene oxide surface to form intermediates (e.g. amide, amine),[35] which can undergo dehydration (e.g. pyridine, pyridone) or decarbonylation (e.g. pyrrole) reactions to form relatively stable structures through the amidation process.[36] The N1 and N2 functionalities increase continuously, further improving the reaction time (8 h, Fig. 4b), simultaneously, N3 components in the XPS spectra also increase, which becomes more obviously when hydrothermal time is increased to 12 h (Fig. 3b) and 16 h (Fig. 4c). This phenomenon is due to the reorganization of unsaturated carbon and N atom incorporation (e.g. pyrrol-N) which may spontaneously occur to form structures of quaternary-N.[23,37] Although the pyrrol-N partly converts to a quaternary-N species, the content of pyrrol-N still increase, which is attributed to the continuous NH$_3$ which could react with the carboxylic acid groups of GO during the hydrothermal reaction.

Recently, carbon materials modified with foreign atoms are the most promising electrode materials since they can enhance capacity by Faradaic reactions in addition to maintaining the superb cycle ability of a supercapacitor.[24] Consequently, NGS as an attractive kind of carbon materials was also used in a supercapacitor. The electrochemical property of the NGS-1 sample was characterized in alkaline media (6 M KOH) by means of a three-electrode cell system. Fig. 5a depicted the cyclic voltammetry (CV) behavior of the NGS-1 at different scan rates, and rectangular voltammetry characteristics could be observed. The appearance of humps in the CV profile is attributed to the contribution of the redox reactions of electrochemically active
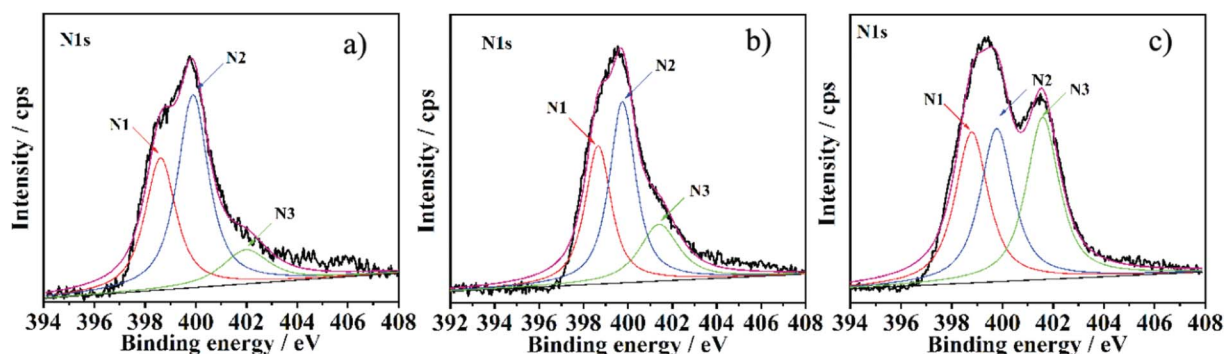

Fig. 4 XPS N1s spectrum of the NGS prepared with different hydrothermal reaction times: a) NGS-9 (4 h), b) NGS-10 (8 h) and c) NGS-11 (16 h).

Scheme 2 a) Nitrogen insertion routes in GO; b) Routes for the formation of a hypothetical structure of quaternary-N in GO.

functional groups on the surface of electrode. Thus, the capacitive response of the NGS is from the combination of EDLC and redox reactions, which is related to the heteroatom functionalities of the carbon materials.[38] The specific capacitance (C_g) of the electrode material was calculated from galvanostatic discharge curves (Fig. 5b). The C_g value for the synthesized NGS-1 is 326 F g^{-1} in 6 M KOH at a current density of 0.2 A g^{-1}, which is much higher than that of the RGO obtained under the same condition (merely 203 F g^{-1} 0.2 A g^{-1}, Table S2, ESI†) and also much higher than that of the other reported carbon-based materials, such as GO-supported conducting polymers[39] and nitrogen-containing carbon materials with high surface area.[40] Fig. 5c presents the relationship between specific capacitance and charge/discharge current density. It is important to note that the C_g value of NGS-1 is still as high as 174 F g^{-1} even at a high current density of 10 A g^{-1}. The superior performance of NGS-1 can be attributed to the high nitrogen level and appropriate nitrogen species, which can provide pseudo-capacitance and lead to excellent electric conductivity. Moreover, the 3D interconnected pore structure and high S_{BET} of NGS-1 are also favorable for the electrolyte penetration and accelerate the kinetic process of the ion diffusion in materials.

The facilitated ion-transport kinetics and electrode conductivity were further confirmed by the electrochemical impedance spectroscopy (EIS). The characteristic impedance curves (Nyquist plots) for the NGS-1 and RGO are shown in Fig. 5d. In the low-frequency region, the slope of the plot for NGS-1 is steeper than RGO, affirming that NGS-1 is characteristic of better capacitive behavior (vertical line for an ideal capacitor).[41]

In the high-frequency region (Fig. 5d inset), the real axis intercept is the equivalent series resistance (ESR), and the radius of semicircle plotted are indicative of electrode conductivity and the charge-transfer resistance in the electrode materials.[42] Notably, the ESR is lower for the NGS-1 than for RGO, and the NGS-1 exhibited a smaller semicircle than RGO. It was concluded that the NGS-1 has a lower charge-transfer resistance and a superb conductivity. The difference in the ion-transport kinetics and electrode conductivity can be attributed to the introduction of nitrogen atoms into graphene. These nitrogen

atoms can not only enhance the surface wettability by electrolytes, but also improve the conductivity of the electrode materials.

Superb cycle stability is crucial to the practical application of supercapacitors. Fig. 6a gives the cycle performance of the NGS-1 electrode investigated by charging/discharging the capacitor for 2000 cycles at a current density of 1 A g^{-1} between −1.1 and −0.1 V. The NGS-1 exhibits outstanding cycling stability and the special capacitance still maintains its initial capacity after 2000 cycles. Most importantly, the coulombic efficiency is maintained at 99.58% after 2000 cycles. The cycling stability of the NGS-1 is further evident from the very stable charge/discharge curves for the last 10 cycles (inset of Fig. 6a). The

Fig. 5 Electrochemical performance of the as-prepared samples using a three-electrode cell in 6 M KOH: a) CV for NGS-1 measured at different scan rate. b) Galvanostatic charge/discharge curves for NGS-1 tested at current density of 0.2–4 A g^{-1}. c) Relationship of the specific capacitance with respect to the charge/discharge specific currents for NGS-1 and RGO. d) Nyquist plots of the NGS-1 and RGO. The inset shows the expanded high-frequency region of the plots. (10 mHz to 100 kHz, ac amplitude, 5 mV).

repetitive charge/discharge cycling does not induce noticeable changes of the structure of NGS-1 nanosheets and the peeling off of NGS-1 from nickel foam does not occur. To investigate the electrochemical performance of NGS-1 at high crucial loads, we further tested the cycling performance at a much larger current density of 5 A g^{-1} and the result is shown in Fig. S6, ESI.† After 6000 cycles, the NGS-1 still retains 99.69% of the initial capacitance with > 99% coulombic efficiency, implying good cycling stability of NGS as electrode materials. In addition, to validate the promising applications of NGS-1 in supercapacitors, a two-electrode symmetric capacitor consisting of a combination of NGS-1 as positive and negative electrodes was constructed by a 2025-type coin cell. The discharge capacity of 56 F g^{-1} can be obtained for this symmetric capacitor at the current density of 1 A g^{-1}. The Ragone plot based on the symmetric supercapacitors in a 6 mol L^{-1} KOH electrolyte is shown in Fig. 6b. The highest energy density of 35.05 Wh kg^{-1} has been achieved at the power density of 175 W kg^{-1} and 25.02 Wh kg^{-1} is retained at a high power density of 7980 W kg^{-1}, which is higher than that of the previous reported carbon-based materials.[38] These results demonstrated that the synthesized NGS materials could be used as promising electrode materials in supercapacitors.

To further investigate the effect of the structure of the NGS on the capacitive behaviors, the electrochemical measurements for all the as-made samples were also performed and the specific capacitances are summarized in Table S2, ESI.† The C_g value for NGS-2, NGS-3, NGS-4 and NGS-5 prepared with different mass ratios between urea and GO are 238, 251, 276, 289 F g^{-1}, respectively, under a current density of 0.2 A g^{-1}. It is concluded that the C_g value increases with the increase in nitrogen content, since the nitrogen functionalities not only afford high pseudo-capacitance, but also prevent aggregation of adjacent graphene sheets.[24,30] Moreover, the capacitive properties of NGS with different hydrothermal temperatures were also studied, and the C_g value for the NGS-6, NGS-7, and NGS-8 are 254, 286 and 281 F g^{-1} under a current density of 0.2 A g^{-1} (Table S2, ESI†), respectively. The test results further reveal the C_g value increases with the improvement of nitrogen level, which could provide electrochemically active nitrogen groups (N1 and N2) and S_{BET}. Hence, the outstanding performance of the NGS-1 electrode should be ascribed to the high nitrogen doping content, proper ratio among each type of nitrogen atoms, and large S_{BET}, which provide the excellent pseudo-capacitance, Superb conductivity, low-resistant pathways and rapid transport of electrolyte ions, respectively.

Based on the above experiment results, it can be presumed that N-type distributions result in the enhanced capacitance in KOH electrolytes, as shown in Fig. 7. It is known that electrochemically active nitrogen atoms (N1 and N2) could easily control local electronic structures, which is beneficial to enhance the band between the N atoms and electrolyte ions of K$^+$ in the solution, resulting in plentiful K$^+$ ions accommodated on the electrode surface.[43] At the same time, the larger number of H$_2$O around the K$^+$ ions was also brought to the electrode surface. In our above experiments (Table S2, ESI†), it is interesting to note that although NGS-4 (S_{BET} = 571 m^2 g^{-1}, N = 8.94 atom%) and NGS-5 (S_{BET} = 544 m^2 g^{-1}, N = 8.45 atom%) have a similar surface area and nitrogen content, the C_g value of NGS-4 (276 F g^{-1}) is lower than that of NGS-5 (289 F g^{-1}). It is
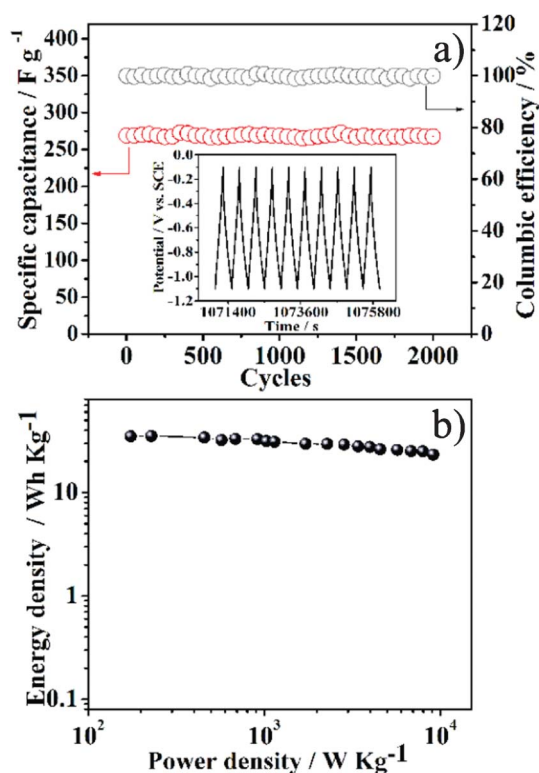

Fig. 6 a) Variations of specific capacitance and the coulombic efficiency *versus* the cycle number of NGS-1 measured at a current density of 1 A g^{-1} within the potential range from −1.1 to −0.1 V. The inset shows the charge–discharge curves of the last 10 cycles for NGS-1. b) Ragone plots of supercapacitors composed of NGS-1 as positive and negative electrodes in 6 M KOH electrolyte.

attributed to the fact that NGS-5 possesses a high amount of the N1 and N2 (7.50 atom%), which can produce redox reactions between H$_2$O and electrochemically active functional groups in graphene. Therefore, the possible oxidation/reduction reaction equation is proposed as followed:

$$-CH = NH + 2e^- + H_2O \leftrightarrows -CH-NHOH$$

Besides, the quaternary-N atoms also play the role of enhancing capacitance by improving the conductivity of the materials, which is favorable to transport electrons in the electrode. It can be seen that the ESR of the NGS materials improves in the order of NGS-5 < NGS-4 < NGS-3 < NGS-2
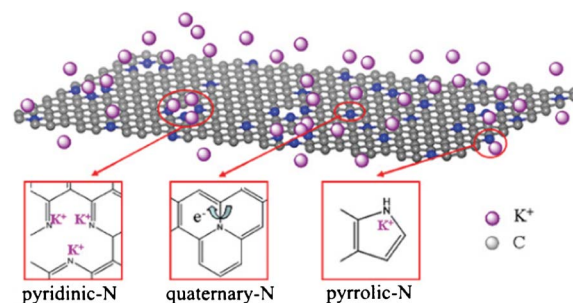

Fig. 7 Scheme of the electrochemical reaction process of NGS materials in 6 M KOH electrolyte.

(Fig. S7, ESI†), indicating that the conductivity of NGS materials can be improved with the increase in the quaternary-N atoms content. The C_g value of NGS-1 is superior to that of NGS-5, attributing to the fact that NGS-1 has abundant electrochemically active nitrogen groups (N1 and N2, 7.32 atom%) raising the pseudo-capacitance, and also has a suitable N3 level (2.77 atom%) which could change the electronic structure of the graphene nanosheets, leading to low-resistant pathways. However, the C_g value of the NGS-4 is lower than that of NGS-5. It can be concluded that although quaternary-N atoms can enhance the conductivity of the NGS materials, the electrochemically active nitrogen groups play a more crucial role in enhancing the energy storage performance. Thus, the high total nitrogen content and the proper ratio among each type of nitrogen atom are very necessary for obtaining high electrochemical performance. It is deduced that the electrochemical properties of the as-prepared samples strongly depend on the nitrogen species due to the pyridinic-N and pyrrolic-N providing pseudo-capacitance by oxidation/reduction reaction, meanwhile the quaternary-N could enhance the conductivity of the materials, which is favourable for electron transfer through the NGS during the charge–discharge process.

4. Conclusions

In summary, a facile and efficient strategy was developed for the fabrication of NGS with a high nitrogen level *via* the hydrothermal reaction of GO with urea. In the procedure, the fact that the urea could release NH_3 is a key factor for the fabrication of NGS with a high nitrogen content. Remarkably, the synthesized NGS-1 sample with both a high nitrogen level (10.13 atom%) and a high surface area (593 m^2 g^{-1}) showed the superb capacitance of 326 F g^{-1} at a current density of 0.2 A g^{-1} in 6 M KOH electrolyte, and also exhibited a good cyclic stability (keeping the initial performance) and coulombic efficient (99.58%) after 2000 cycles. Most importantly, the energy density is up to 25.02 Wh kg^{-1} at the power density of 7980 W kg^{-1} by two-electrode symmetric capacitor tests. The outstanding performance should be ascribed to the high nitrogen doping content, proper ratio among each type of nitrogen atoms, and large surface area, which can be provided the high pseudo-capacitance, well conductivity, low-resistant pathways and rapid transport of electrolyte ions, respectively. It was demonstrated that the synthesized NGS samples could be used as a kind of promising electrode materials for high-performance supercapacitors.

Acknowledgements

References

1 J. R. Miller and P. Simon, *Science*, 2008, **321**, 651.
2 C. Liu, F. Li, L. P. Ma and H. M. Cheng, *Adv. Mater.*, 2010, **22**, E28.
3 P. Simon and Y. Gogotsi, *Nat. Mater.*, 2008, **7**, 845.
4 (*a*) W. T. Deng, X. B. Ji, Q. Y. Chen and C. E. Banks, *RSC Adv.*, 2011, **1**, 1171; (*b*) C. C. Hu, K. H. Chang, M. C. Lin and Y. T. Wu, *Nano Lett.*, 2006, **6**, 2690.
5 S. Chen, J. W. Zhu, H. Zhou and X. Wang, *RSC Adv.*, 2011, **1**, 484.
6 D. Aradilla, F. Estrany and C. Alemán, *J. Phys. Chem. C*, 2011, **115**(16), 8430.
7 H. Zhu, X. L. Wang, F. Yang and X. R. Yang, *Adv. Mater.*, 2011, **24**, 2745.
8 H. Zhang, G. P. Cao and Y. S. Yang, *Energy Environ. Sci.*, 2009, **2**, 932.
9 S. H. Aboutalebi, A. T. Chidembo, M. Salari, K. Konstantinov, D. Wexler, H. K. Liu and S. X. Dou, *Energy Environ. Sci.*, 2011, **4**, 1855.
10 Y. P. Zhai, Y. Q. Dou, D. Y. Zhao, P. F. Fulvio, R. T. Mayes and S. Dai, *Adv. Mater.*, 2011, **23**, 4828–4850.
11 D. S. Yuan, J. X. Chen, J. X. Chen, S. X. Tan, N. N. Xia and Y. L. Liu, *Electrochem. Commun.*, 2009, **11**, 1191.
12 Z. Chen, J. Wen, C. Z. Yan, L. Rice, H. Sohn, M. Q. Shen, M. Cai, B. Dunn and Y. F. Lu, *Adv. Energy Mater.*, 2011, **1**, 551.
13 M. Kaempgen, C. K. Chan, J. Ma, Y. Cui and G. Gruner, *Nano Lett.*, 2009, **9**, 1872.
14 A. K. Geim, *Science*, 2009, **324**, 1530.
15 M. D. Stoller, S. Park, Y. Zhu, J. An and R. S. Ruoff, *Nano Lett.*, 2008, **8**, 3498.
16 H. M. Jeong, J. W. Lee, W. H. Shin, Y. J. Choi, H. J. Shin, J. K. Kang and J. W. Choi, *Nano Lett.*, 2011, **11**, 2472.
17 Y. C. Qiu, X. F. Zhang and S. H. Yang, *Phys. Chem. Chem. Phys.*, 2011, **13**, 12554.
18 Z. Y. Jin, J. C. Kittrell and J. M. Tour, *ACS Nano*, 2011, **5**, 4112.
19 L. S. Panchokarla, K. S. Subrahmanyam, S. K. Saha, A. Govindaraj, H. R. Krishnamurthy, U. V. Waghmare and C. N. R. Rao, *Adv. Mater.*, 2009, **21**, 4726.
20 Y. Wang, Y. Y. Shao, D. W. Matson, J. H. Li and Y. H. Lin, *ACS Nano*, 2010, **4**, 1790.
21 X. R. Wang, X. L. Li, L. Zhang, Y. K. Yoon, P. K. Weber, H. L. Wang, J. Guo and H. J. Dai, *Science*, 2009, **324**, 768.
22 X. L. Li, H. L. Wang, J. T. Robinson, H. Sanchez, G. Diankov and H. J. Dai, *J. Am. Chem. Soc.*, 2009, **131**, 15939.
23 (*a*) D. H. Long, W. Li, L. C. Ling, J. Miyawaki, I. Mochida and S. H. Yoon, *Langmuir*, 2010, **26**(20), 16096; (*b*) H. Deng, X. L. Pan, L. Yu, Y. Cui, Y. P. Jiang, J. Qi, W. X. Li, Q. Fu, X. C. Ma, Q. K. Xue, G. Q. Sun and X. H. Bao, *Chem. Mater.*, 2011, **23**(5), 1188.
24 D. Hulicova-Jurcakova, M. Seredych, G. Q. Lu and T. J. Bandosz, *Adv. Funct. Mater.*, 2009, **19**, 438.
25 L. Wei, M. Sevilla, A. B. Fuertes, R. Mokaya and G. Yushin, *Adv. Energy Mater.*, 2011, **1**, 356.
26 Z. H. Sheng, L. Shao, J. J. Chen, W. J. Bao, F. B. Wang and X. H. Xiao, *ACS Nano*, 2011, **6**, 4350.
27 H. L. Wang, J. T. Robinson, X. L. Li and H. J. Dai, *J. Am. Chem. Soc.*, 2009, **131**, 9910.
28 G. L. Wang, J. C. Huang, S. L. Chen, Y. Y. Gao and D. X. Cao, *J. Power Sources*, 2011, **196**, 5756.
29 Y. W. Zhu, S. T. Murali, M. D. Stoller, K. J. Ganesh, W. W. Cai, P. J. Ferreira, A. Pirkle, R. M. Wallace, K. A. Cychosz, M. Thommes, D. Su, E. A. Stach and R. S. Ruoff, *Science*, 2011, **332**, 1537.
30 Z. Y. Lin, Y. Liu, Y. G. Yao, O. J. Hildreth, Z. Li, K. Moon and C. P. Wong, *J. Phys. Chem. C*, 2011, **115**(14), 7120.
31 J. P. Pels, F. Kapteijn, J. A. Moulijn, Q. Zhu and K. M. Thomas, *Carbon*, 1995, **33**, 1641.
32 A. J. Patil, J. L. Vickery, T. B. Scott and S. Mann, *Adv. Mater.*, 2009, **21**, 3159.
33 D. C. Wei, Y. Q. Liu, Y. Wang, H. L. Zhang, L. P. Huang and G. Yu, *Nano Lett.*, 2009, **9**, 1752.
34 C. Malitesta, I. Losito, L. Sabbatini and P. G. Zambonin, *J. Electron Spectrosc. Relat. Phenom.*, 1995, **76**, 629.
35 R. Arrigo, M. Hävecker, S. Wrabetz, R. Blume, M. Lerch, J. McGregor, E. P. J. Parrott, J. A. Zeitler, L. F. Gladden, A. Knop-Gericke, R. Schlögl and D. S. Su, *J. Am. Chem. Soc.*, 2010, **132**(28), 9616.
36 S. Stankovich, D. A. Dikin, R. D. Piner, K. A. Kohlhaas, A. Kleinhammes, Y. Jia, Y. Wu, S. T. Nguyen and R. S. Ruoff, *Carbon*, 2007, **45**, 1558.
37 R. Arrigo, M. Hävecker, R. Schlögl and D. S. Su, *Chem. Commun.*, 2008, **40**, 4891.

38 H. Zhu, X. L. Wang, F. Yang and X. R. Yang, *Adv. Mater.*, 2011, **23**, 2745.

39 E. Frackowiak, G. Lota, J. Machnikowski, C. Vix-Guterl and F. Béguin, *Electrochim. Acta*, 2006, **51**, 2209.

40 L. Zhao, L. Fan, Z. Zhou, M. Q. Guan, H. Qiao, S. M. Antonietti and M. M. Titirici, *Adv. Mater.*, 2011, **22**, 5202.

41 G. P. Pandey, S. A. Hashmi and Y. Kumar, *J. Electrochem. Soc.*, 2010, **157**, A105.

42 G. P. Pandey, S. A. Hashmi and Y. Kumar, *Energy Fuels*, 2010, **24**, 6644.

43 R. I. Jafri, N. Rajalakshmi and S. Ramaprabhu, *J. Mater. Chem.*, 2010, **20**, 7114.